Nanoscale

Accepted Manuscript

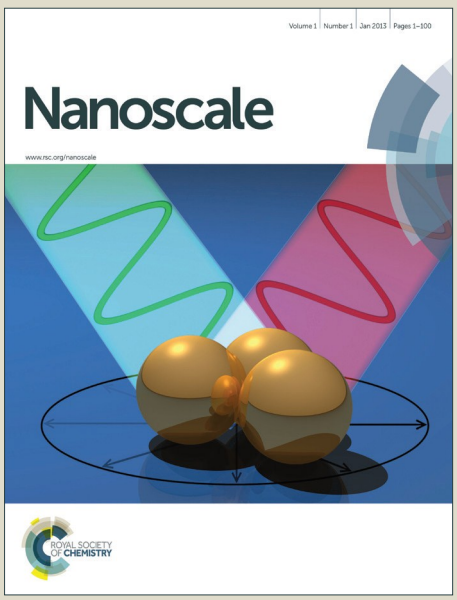

ROYAL SOCIETY OF CHEMISTRY

www.rsc.org/nanoscale

Fracture Patterns and Energy Release Rate of Phosphorene

Ning Liu [1], Jiawang Hong [2], Ramana Pidaparti [1*] and Xianqiao Wang [1*]

[1] College of Engineering, University of Georgia, Athens, GA 30602

[2] Materials Science and Technology Division, Oak Ridge National Laboratory, Oak Ridge, TN 37830

* Joint corresponding authors: xqwang@uga.edu and rmparti@uga.edu

Abstract

Phosphorene, also known as monolayer black phosphorous, has been enjoying the popularity in electronic devices due to its superior electrical properties. However, it's relatively low Young's modulus, low fracture strength and susceptibility to structural failure has limited its application in mechanical devices. Therefore, in order to design more mechanically reliable devices that utilize phosphorene, it is necessary to explore the fracture patterns and energy release rate of phosphorene. In this study, molecular dynamics simulations are performed to investigate phosphorene's fracture mechanism. Results indicate that fracture under uniaxial tension along the armchair direction is attributed to a break in the interlayer bond angles, while failure in the zigzag direction is triggered by the break in both the intra-layer angles and bonds. Furthermore, we developed a modified Griffith criterion to analyze the energy release rate of phosphorene and its dependence on strain rates and orientations of cracks. Simulation results indicate that phosphorene's energy release rate remains almost unchanged in the armchair direction while it fluctuates intensively in the zigzag direction. Additionally, the strain rate was found to play a negligible role in the energy release rate. The geometrical factor α in the Griffith's criterion is almost constant when the crack orientation is smaller than 45 degree, regardless of the crack orientation and loading direction. Overall, these findings provide helpful insights into the mechanical properties and failure behavior of phosphorene.

Introduction

In recent years, great efforts have been made to discover new two-dimensional layered materials since the successful fabrication of graphene[1, 2], including silicene[3], hexagonal boron nitride (h-BN)[4, 5] and transition metal dichalcongenide[6]. Phosphorene, a counterpart of bulk black phosphorous as a novel 2D material, has recently been another hot topic in material science. Through mechanical methods, phosphorene with few layers[7] or even a single layer[8] has already

been exfoliated. Due to its unique physical properties, such as a finite and direct band gap[9] and high free carrier mobility[10], phosphorene has been explored as a new two-dimensional material for applications in nanoelectronic devices. Moreover, with a puckered structure, phosphorene exhibits various unique mechanical properties, such as negative Poisson's ratio[11] and anisotropic ripple deformation[12]. Despite the outstanding physical properties, phosphorene is easily affected by the environment[13 14 15 16]. Kou et al systematically study the absorption of multiple kinds of gas molecules, including CO, CO_2, NH_3, NO and NO_2, by first-principle calculations, the results of which reveal that phosphorene is more sensitive to these nitrogen-based molecules, such as NO and NO_2[14]. In terms of the applications of phosphorene, a key issue related to the fracture patterns and relevant fracture strength of phosphorene has to be solved in order to clearly understand its reliability in the devices. Despite advances that have been made in studying phosphorene's mechanical properties by DFT, the fracture patterns and energy release rate of phosphorene remains largely unexplored. Compared with DFT, molecular dynamics (MD) is an ideal method for studying the fracture properties of phosphorene due to its high computational efficiency and the relatively large simulation system. A Stillinger–Weber (SW) potential has been recently proposed by Jiang to accurately predict the mechanical properties of phosphorene. He found that phosphorene has high anisotropy in fracture strain, fracture stress and Young's Modulus[17]. These findings have also been confirmed by other investigations adopting this potential[18 19].However, the mechanism of high anisotropy still remains unclear. Therefore, in this study, molecular simulations are performed to understand the mechanism underlying different mechanical properties along the armchair and zigzag directions, including fracture patterns.

The validity and the feasibility of linking the atomistic information of a material of interest from molecular dynamics simulations to its macroscopic material properties via conventional continuum theory is always an interesting topic, especially for those novel 2D materials. [20-22] Previous studies have explored the usability of continuum theory for analyzing the mechanical and fracture behaviors of graphene. For example, the breakdown of continuum fracture mechanics, energy release rate and Griffith criterion, has been observed in graphene sheets by molecular dynamics simulations when the crack length is below 2-3 nm[23]. Furthermore, a new analytic theory, named discrete fracture mechanics (DFM) has emerged for studying the energy release rate, which shows its validity at both the nanoscale and macroscale. The applicability of the classic Griffith theory of brittle fracture has been verified by measuring the fracture

toughness of graphene through *in situ* tensile testing as the initial crack length ranges from 33nm to 1,256nm [24]. Lopez-polin et al. conducted a systematic study on the dependence of the elastic modulus and the strength of graphene on the density of defects[25]. A fracture mechanics framework based on Griffith criterion was proposed, which showed that the fracture strength is proportional to the inverse of the square root of vacancy percentage. Tsai et al. characterized the energy release rate of a graphene sheet adopting both molecular dynamics simulations and continuum finite element analysis, and proved that energy release rate is an appropriate parameter in predicting the fracture behaviors of graphene sheets[26]. A recent investigation suggested that the Griffith criterion, a fundamental theory for determining the fracture toughness, is not valid any more in graphene with cracks shorter than 10nm[27]. Consequently, a modified criterion has been proposed to accurately describe the fracture patterns of models with cracks shorter than 10nm in graphene. However, the applicability of the Griffith facture criterion to phosphorene remains unclear. This study will focus on the investigation of the fracture patterns and energy release rate of phosphorene using molecular dynamics simulations and propose a modified Griffith criterion based on the results of fracture mechanics to study the geometrical factors.

Computational Methodology and Models

Figure 1 shows the geometrical configuration for phosphorene, which has already been identified and verified by experiments. Figure 1(a) is a perspective view, indicating that unlike other 2D materials such as graphene, phosphorene has an in-plane puckered structure. Phosphorous atoms are distributed on the top layer and bottom layer respectively, as shown in Figure 1(b).The unit cell of phosphorene is composed of four atoms as shown in Figure 1(d), in which $\overrightarrow{a_1}$ and $\overrightarrow{a_2}$ are basis vectors along the armchair and zigzag directions, respectively. According to Jiang et al.[17], the lengths of $\overrightarrow{a_1}$ and $\overrightarrow{a_2}$ are 4.36 and 3.31Å (10^{-10}m), respectively.

In this study, molecular dynamics simulations are performed with an open source package LAMMPS based on the Stillinger-Weber (SW) potential developed by Jiang et al[17]. SW potential was initially developed for bulk silicon systems[28], but has been successfully extended to many other materials such as molybdenum disulphide (MoS_2)[29] and wurtzite GaN[30]. While many different kinds of force fields exist for 2D materials and structures, for example AIREBO [31] and ReaxFF [32] for graphene, Tersoff [33] for silicence etc., to the best of our knowledge for

phosphorene the Stillinger-Weber potential form is the only type of interatomic potentials now available in literatures [17 34 35]. It consists of two terms, a two-body term representing the bond stretching interaction and a three-body term representing the bond bending interaction, and is expressed as follows.

$$\emptyset = \sum_{i<j} V_2 + \sum_{i<j<k} V_3 \quad (1)$$

$$V_2 = \varepsilon A\left(B\sigma^p r_{ij}^{-p} - \sigma^q r_{ij}^{-q}\right)e^{\left[\sigma(r_{ij}-a\sigma)^{-1}\right]} \quad (2)$$

$$V_3 = \varepsilon\lambda e^{\left[\Upsilon\sigma(r_{ij}-a\sigma)^{-1}+\Upsilon\sigma(r_{jk}-a\sigma)^{-1}\right]}(cos\theta_{ijk} - cos\theta_0)^2 \quad (3)$$

where V_2 and V_3 are the two-body term and three body term respectively; r_{ij} is the distance between atom i and j; Θ_{ijk} is the angle between bond ij and bond jk; Θ_0 is the equilibrium angle between two bonds; all the other parameters such as A, B are the coefficients required to fit when developing the potential.

Due to the geometrical configuration of phosphorene as shown in Figure 1(f), two types of atoms are defined in the SW potential. The red atoms in the figure represent the top layer atoms while the blue atoms represent the bottom layer atoms. Hence there are two types of bonds, namely interlayer bonds and intralayer bonds. Bonds connecting atoms in the same layer are called intralayer bonds, while those connecting atoms in different layers are called interlayer bonds. However, the parameters are the same for these two types of bonds as pointed out by Jiang et al[17]. With respect to the three-body term in the SW potential, two types of bond angles are defined. A bond angle is categorized as an intralayer angle if all bonds involved are interlayer bonds, while the bond angle established by bonds of different types is an interlayer bond angle. The balance values of intralayer and interlayer angles are 96.359° and 102.09°, respectively. All the parameters for the SW potential are shown in Table 1[17].

A rectangle with 26.2×19.9 nm^2 is considered as the initial model of phosphorene in MD simulations (there are 14,400 atoms totally in a pristine model). A predefined crack is introduced by deleting atoms along a certain direction. Crack orientation Θ is defined as the angle between the crack and the direction perpendicular to the external loading as shown in Figure 1(e). In this study, Θ is considered as being 0°, 15°, 30°, 45°, 60° or 75°, while the crack length is chosen as 2,

3, 4, 5 or 6 nm. Period boundary conditions are adopted along the in-plane directions while a free boundary is used in the out-of-plane direction. Before tensile tests are performed, an energy minimization process using the conjugated gradient method is performed. Then in order to stabilize the temperature and pressure of the system, NPT and NVT ensembles are run for 40,000 steps each, alternatively for 4 rounds. The time step in the simulation is set as 1fs.The whole system is kept at 1K during these periods. After a long period of equilibration, the NPT ensemble is adopted to do the tensile test with the same time step and environmental temperature. During the tensile test, the model is elongated by 0.001 strains every 10,000 steps along the loading direction.

Results and Discussions

Failure mechanism

Due to its unique electrical properties, phosphorene has shown a great potential for use in nanoelectronic devices. However, a key issue related to the fracture patterns and relevant fracture toughness of phosphorene has to be solved in order to clearly understand its reliability in these devices. Therefore, to understand its fracture mechanism, a series of tensile tests are performed in both the armchair and zigzag directions. First, pristine models are used in the uniaxial tension along both the armchair and zigzag directions, with the stress-strain curves shown in Figure 2.

Young's Modulus of the phosphorene is obtained by linear fitting of the stress versus strain when the strain is below 0.02. The magnitudes of Young's modulus for both the armchair and zigzag directions are 24.28GPa and 103.83GPa respectively, and are in good agreement with the 20.9GPa and 90.5GPa obtained from a recent investigation[18]. Moreover, the fracture stress for both armchair and zigzag directions is 3.94GPa and 7.95Gpa while the fracture strain is 0.295 and 0.161 for the armchair and zigzag directions respectively. Note that our results about Young's modulus are at least 10% higher than that from the literature[18], which is caused by the temperature difference. The Young's moduli in our manuscript are calculated from the uniaxial tensile tests when temperature is 1 K, while the counterpart results from Sha et al[18] are simulated under 300 K. The dependence of mechanical properties on temperature is investigated and the detailed information can be found in Figure S1 and Table S1 (see Supporting Information).

Results indicate that as the temperature increases, both Young's modulus and fracture stress decreases.

To determine the mechanism of the difference in critical fracture strain under uniaxial tensile tests along different directions, the maximum bond length is plotted as a function of strain for both armchair direction and zigzag direction in Figure 3(a). For the armchair direction tension, the maximum length of interlayer bonds undergoes larger changes than that of intralayer bonds, while for zigzag direction tension the maximum length of intralayer bonds experience larger changes. Therefore, interlayer bonds are the dominating bonds for the armchair direction tension while intralayer bonds are dominating bonds under the zigzag direction tension. These dominating bonds under the zigzag direction tension increase much faster than those under the armchair direction, leading to a smaller fracture strain under the zigzag direction tension. Note that as the maximum length of dominating bonds arrives at a critical value, 0.2362nm for pristine models, these dominating bonds with the maximum length undergo a sudden length change accompanied by the nucleation of a crack. Figure 3(b) shows the average change of potential energy increase for both the armchair and zigzag directions. As we can see, under the armchair direction tension, the average energy change of bonds and angles increases slower than that under the zigzag direction tension. Therefore, a slower change of bond energy and angle energy makes the armchair direction of phosphorene more flexible than the zigzag direction under the uniaxial tension, namely a lower Young's Modulus. Figure 3(b) also indicated that the average total energy change along the zigzag direction is slightly higher than that along the armchair direction while the fracture strain along the zigzag direction is much less than that along the armchair direction, leading to a higher fracture stress along the zigzag direction.

Note that there are a lot of fluctuations in the stress-strain curve during armchair direction tension. To explain why this phenomenon occurs during uniaxial tension along the armchair direction, the average angle change and bond length change are plotted as a function of strain in Figure 4. From the figure, we can notice that the average change of interlayer angles is much larger than that of intralayer angles. Moreover, fluctuations are observed in the curve of intralayer angle change while there are no obvious fluctuations in the curve of interlayer angle change. Figure 4 also shows that at the beginning of the deformation, the average length change of interlayer bonds is close to that of intralayer ones while this trend breaks down after the strain

becomes larger than 0.05. After the critical strain 0.05, the average length of interlayer bond changes faster than that of intralayer bond. Again fluctuations are observed on the curve of the average length change of intralayer bonds. Based on results presented in Figure 4, a conclusion can be drawn that the fluctuations of the stress-strain curve in armchair tension are caused by the vibration of intralayer angles and bonds.

Figure 5 shows the average energy change under uniaxial tension along the armchair direction of a phosphorene model with a 2nm crack. It can be seen from the figure that the increase in potential energy is mainly caused by the increase in interlayer angle energy, which means that the fracture of the phosphorene sheet is caused by a break in the interlayer angle. The break in the interlayer angles is caused by the break in the bonds involved in the group while the bond type is unknown since there are two types of bonds involved. Note that there is permanent change in total energy compared to the initial state, which is almost same as the interlayer bond energy change. The increased energy is the surface energy created by the fracture. Therefore, it is the break in the interlayer bonds that caused the break in the interlayer angles, resulting in the propagation of cracks. This is also confirmed by the snapshots of crack progress as shown in Figure 6.

Figure 7 shows the average energy change under uniaxial tension along the zigzag direction of a phosphorene model with a 2nm crack. The average energy increase in intralayer bonds is comparable to that of intralayer angles, while the average energy change in interlayer bonds and angles is negligible. Therefore, the fracture under tension along zigzag direction is caused by the break in the intralayer bonds and angles. Figure 8 shows the snapshots of the fracture process, which indicate the crack path is perpendicular to the loading direction without any kinks. During the propagation of cracks, the interlayer bonds and angles are broken, which reconfirms the above finding.

Energy release rate

Energy release rate is a widely used parameter to measure fracture strength in linear elastic fracture mechanics, which typically take it for granted as a material constant. However, for materials at the nanoscale like graphene, the energy release rate has been demonstrated to no longer be a constant, depending on the crack orientation, the configuration of the crack tip, and

other structural parameters[27]. For phosphorene, energy release rate remains largely unexplored. Therefore, a series of simulations are performed to calculate the energy release rate of phosphorene with cracks along different orientations. The methodology proposed by Zhang et al.[36] is adopted as follows to calculate the energy release rate G_c

$$G_c = -\frac{dW}{2t \times da} = \frac{W_a - W_{a+\Delta a}}{2t \times \Delta a} \quad (4)$$

where W_a and $W_{a+\Delta a}$ indicates the total external work required for models with initial crack lengths a and $a + \Delta a$ to drive the propagation of the crack respectively, while t is the thickness of the model. Here an interlayer separation distance of 0.524nm, is defined as the effective thickness t. The external work is calculated from the stress-strain curves as shown in Figure 9. For each crack orientation Θ, 5 samples with different initial crack lengths are used to obtain an average value of the energy release rate. Note that as the crack length changes, Young's modulus changes accordingly. This is because the pre-existing cracks weaken the phosphorene layer, making it softer than pristine models. As the length of the crack becomes larger, the softening effect becomes more obvious.

Figure 10 shows the energy release rate as a function of crack orientation Θ for both armchair direction and zigzag directions. It is important to note that that energy release rate of phosphorene is very comparable with that of graphene[27]. Interestingly, energy release rates for specimens with different crack orientation are very close to each other under the armchair direction, while under the zigzag direction, energy release rates vary largely with the crack angle, ranging from 5.66 to 16.66 J/m^2. The obtained data points are fitted into a linear form. The slope of the armchair direction is 0.0261 $J/(m^2.degree)$, which is smaller than the value of the slope in the zigzag direction, 0.1258 $J/(m^2.degree)$.The high anisotropy with respect to energy release rate results from the puckered structure in the armchair direction.

The proceeding simulations are all performed at a constant strain rate $1 \times 10^{-3}\text{ps}^{-1}$. An intriguing question as to whether the strain rate plays a vital role in the energy release rate of phosphorene remains unanswered. To understand the relationship between these two parameters, computational tests are carried out for phosphorene with initial cracks perpendicular to the loading direction under different strain rates, ranging from 5×10^{-5} to $1 \times 10^{-3}\text{ps}^{-1}$. Both zigzag and armchair directions are selected as loading directions. The energy release rate is

shown as a function of strain rate in Figure 11, where the red line and blue line represent fitting results of energy release rate for armchair and zigzag direction respectively while the blue dots and red stars represent original data. From Figure 11, we are able to infer that strain rates probably play a negligible role in determining energy release rate for phosphorene for both zigzag and armchair directions. This finding is in accordance with a recent investigation on the fracture properties of graphene. According to the study[37], when the temperature is 300K, despite the great variation of strain rate, from 5×10^{-5} to $5 \times 10^{-3}\text{ps}^{-1}$, the increase in fracture strength is only 4% for single crystalline graphene. In classical fracture mechanics, the fracture process must be treated as a dynamic one, where the following influences cannot be neglected: rate-dependent material behavior, inertia forces, and reflected stress waves[38]. However, according to our previous findings, phosphorene is not a kind of material with rate-dependent behaviors. Moreover, in our case, the atoms are mapped to new positions every N steps, without incorporating new velocities and accelerations. On the other hand, the temperature is maintained at 1 Kelvin, so the random motions of the atoms are relatively moderate. Therefore, the influence of inertia forces and reflected stress waves can be neglected. In summary, the cases simulated in this paper can be viewed as quasi-static fracture.

Modified Griffith Criterion

Griffith criterion is another widely used concept to measure fracture strength in linear elastic fracture mechanic. Since this theory is developed under the assumption of macroscale system, its applicability in nanoscale materials remains uncertain. For 2D materials like graphene, its fracture behavior has been explored and it has been concluded that the breakdown of Griffith criterion occurs when the crack length is below 10nm[27]. Our simulations are all performed in samples with predefined cracks less than 10nm in length. Following the finding with graphene, we propose here a new fracture criterion for phosphorene with an effective geometrical correction α as follows,

$$\sigma_f = \alpha \frac{1}{F(\emptyset)} \sqrt{\frac{EG_c}{\pi a}} \tag{5}$$

where σ_f is the fracture stress, G_c is the energy release rate and E is Young's modulus. According to Yin et al[27], $F(\Phi)$ is a geometrical factor given by

$$F(\emptyset) = 1 - 0.025\emptyset^2 + 0.06\emptyset^4\sqrt{\sec\left(\frac{\pi\emptyset}{2}\right)}, and\ \emptyset = \frac{Wid}{2a} \quad (6)$$

where Wid is the width of the stripe with a central crack of length $2a$. Geometrical correction α, is 3 for graphene sheets with initial cracks shorter than 10nm. However, the applicability of this criterion in phosphorene remains unproven yet. To verify this criterion, the critical stress is fitted to equation (5). Note that the relationship between σ_f and $\frac{1}{F(\Phi)\sqrt{a}}$ is not proportional but linear, meaning there should be a constant added to the end of the right side of equation 6.

Figure 12 shows fracture stresses versus crack length when crack orientation is 30 degree for both armchair and zigzag direction, where blue dots represent the original data and blue lines represent the fitting results. Detailed information about Griffith criterion for all other crack orientations can be found in the Supporting Information. Furthermore, the geometrical factors α are obtained for different crack orientations for both armchair and zigzag unidirectional tensions, which are summarized in Table 2. In the current investigation, the crack orientation varies from 0 to 75 degree, while in the investigation about graphene[27], the crack orientation ranges from 0 to 30 degree. When the degree of crack orientation is bigger than 30 degree, the variance of geometrical factor for graphene is still unknown. For phosphorene, when the degree of the crack orientation is smaller than 45, the geometrical factor fluctuates around 0.227 and 0.222 for both armchair and zigzag directions respectively as shown in Table 2. We think the geometrical factor for phosphorene follows the pattern of graphene as a constant. However, when the crack orientation is bigger than 45 degree, 60 and 75 degree in the present paper, the fracture becomes less sensitive to the crack length. Therefore, the geometrical factor becomes smaller as the degree of crack orientation becomes bigger in this regime. The detailed information for all crack orientations including 60 and 75 degree can be found in the Figure S2, Figure S3 and Table S2 from the Supporting Information.

Concluding remarks

In this study, we performed a series of molecular dynamics simulations to study the fracture patterns, energy release rate, and the applicability of Griffith criterion to phosphorene. Results revealed that phosphorene is brittle and anisotropic in fracture strain, Young's modulus and fracture strength. The fracture strain is bigger in the armchair direction than in the zigzag

direction because of the slower bond length change rate under tension, which is caused by its unique puckered structure. Compared with the zigzag direction, the smaller Young's Modulus in the armchair direction is caused by the slower change rate in the bond energy and angle energy. For the armchair direction, the fracture strength is much weaker than that in the zigzag direction, resulting from the comparable potential energy change but smaller fracture strain compared with the zigzag direction. With respect to energy release rate, when the crack orientation θ changes, the variation in the armchair direction is small while the fluctuation in the zigzag direction is very large. Moreover, the influence of strain rate on the energy release rate can be neglected. We also verified the applicability of the modified Griffith criterion proposed by Yin et al[27]. Results indicate that this model effectively describes the relations between fracture stress and initial crack length. Furthermore, the geometrical factor α is found to almost remain a constant when the crack orientation is smaller than 45 degree.

Acknowledgement

XW acknowledge supports from the National Science Foundation (Grant No. CMMI-1306065) and the University of Georgia (UGA) Research Foundation. Calculations are performed at the UGA Advanced Computing Resource Centre.

References

1. K. S. Novoselov, A. K. Geim, S. V. Morozov, D. Jiang, Y. Zhang, S. V. Dubonos, I. V. Grigorieva and A. A. Firsov, *Science*, 2004, **306**, 666-669.
2. L. Zhang, X. Zeng and X. Wang, *Sci Rep*, 2013, **3**, 3162.
3. P. Vogt, P. De Padova, C. Quaresima, J. Avila, E. Frantzeskakis, M. C. Asensio, A. Resta, B. Ealet and G. Le Lay, *Phys. Rev. Lett.*, 2012, **108**, 5.
4. L. Song, L. Ci, H. Lu, P. B. Sorokin, C. Jin, J. Ni, A. G. Kvashnin, D. G. Kvashnin, J. Lou, B. I. Yakobson and P. M. Ajayan, *Nano Letters*, 2010, **10**, 3209-3215.
5. X. Chen, L. Zhang, C. Park, C. C. Fay, X. Wang and C. Ke, *Applied Physics Letters*, 2015, **107**, 253105.
6. Q. H. Wang, K. Kalantar-Zadeh, A. Kis, J. N. Coleman and M. S. Strano, *Nat. Nanotechnol.*, 2012, **7**, 699-712.
7. L. Li, Y. Yu, G. J. Ye, Q. Ge, X. Ou, H. Wu, D. Feng, X. H. Chen and Y. Zhang, *Nat Nano*, 2014, **9**, 372-377.

8. H. Liu, A. T. Neal, Z. Zhu, Z. Luo, X. F. Xu, D. Tomanek and P. D. D. Ye, *ACS Nano*, 2014, **8**, 4033-4041.
9. X. H. Peng, Q. Wei and A. Copple, *Phys. Rev. B*, 2014, **90**, 10.
10. B. L. Liao, J. W. Zhou, B. Qiu, M. S. Dresselhaus and G. Chen, *Phys. Rev. B*, 2015, **91**, 8.
11. J.-W. Jiang and H. S. Park, *Nat Commun*, 2014, **5**.
12. L. Kou, Y. Ma, S. C. Smith and C. Chen, *The Journal of Physical Chemistry Letters*, 2015, **6**, 1509-1513.
13. L. Kou, C. Chen and S. C. Smith, *The Journal of Physical Chemistry Letters*, 2015, **6**, 2794-2805.
14. L. Kou, T. Frauenheim and C. Chen, *The Journal of Physical Chemistry Letters*, 2014, **5**, 2675-2681.
15. C.-G. Andres, V. Leonardo, P. Elsa, O. I. Joshua, K. L. Narasimha-Acharya, I. B. Sofya, J. G. Dirk, B. Michele, A. S. Gary, J. V. Alvarez, W. Z. Henny, J. J. Palacios and S. J. v. d. Z. Herre, *2D Materials*, 2014, **1**, 025001.
16. J. Dai and X. C. Zeng, *RSC Adv.*, 2014, **4**, 48017-48021.
17. J. Jin-Wu, *Nanotechnology*, 2015, **26**, 315706.
18. S. Zhen-Dong, P. Qing-Xiang, D. Zhiwei, J. Jin-Wu and Z. Yong-Wei, *Journal of Physics D: Applied Physics*, 2015, **48**, 395303.
19. Z. Y. Yang, J. H. Zhao and N. Wei, *Applied Physics Letters*, 2015, **107**, 5.
20. X. Chen, L. Zhang, Y. Zhao, X. Wang and C. Ke, *Journal of Applied Physics*, 2014, **116**, 164301.
21. L. Zhang, M. Becton and X. Wang, *Materials Science and Engineering: A*, 2015, **620**, 367-374.
22. L. Zhang and X. Wang, *Phys Chem Chem Phys*, 2014, **16**, 2981-2988.
23. T. Shimada, K. Ouchi, Y. Chihara and T. Kitamura, *Scientific Reports*, 2015, **5**, 8596.
24. P. Zhang, L. Ma, F. Fan, Z. Zeng, C. Peng, P. E. Loya, Z. Liu, Y. Gong, J. Zhang, X. Zhang, P. M. Ajayan, T. Zhu and J. Lou, *Nat Commun*, 2014, **5**.
25. G. Lopez-Polin, C. Gomez-Navarro, V. Parente, F. Guinea, M. I. Katsnelson, F. Perez-Murano and J. Gomez-Herrero, *Nat. Phys.*, 2015, **11**, 26-31.
26. J.-L. Tsai, S.-H. Tzeng and Y.-J. Tzou, *International Journal of Solids and Structures*, 2010, **47**, 503-509.
27. H. Yin, H. J. Qi, F. Fan, T. Zhu, B. Wang and Y. Wei, *Nano Letters*, 2015, **15**, 1918-1924.
28. F. H. Stillinger and T. A. Weber, *Phys. Rev. B*, 1985, **31**, 5262-5271.
29. J.-W. Jiang, H. S. Park and T. Rabczuk, *J. Appl. Phys.*, 2013, **114**, 064307.

30. Z. Liang, A. Jain, A. J. H. McGaughey and P. Keblinski, *J. Appl. Phys.*, 2015, **118**, 125104.

31. S. J. Stuart, A. B. Tutein and J. A. Harrison, *The Journal of Chemical Physics*, 2000, **112**, 6472-6486.

32. A. C. T. van Duin, S. Dasgupta, F. Lorant and W. A. Goddard, *The Journal of Physical Chemistry A*, 2001, **105**, 9396-9409.

33. B. Virgile, H. T. Diep, E. Hanna, O. Hamid and K. Addelkader, *Journal of Physics: Conference Series*, 2014, **491**, 012008.

34. W. Xu, L. Y. Zhu, Y. Q. Cai, G. Zhang and B. W. Li, *J. Appl. Phys.*, 2015, **117**, 7.

35. J. W. Jiang, T. Rabczuk and H. S. Park, *Nanoscale*, 2015, **7**, 6059-6068.

36. Z. Zhang, X. Wang and J. D. Lee, *J. Appl. Phys.*, 2014, **115**, 114314.

37. M. Q. Chen, S. S. Quek, Z. D. Sha, C. H. Chiu, Q. X. Pei and Y. W. Zhang, *Carbon*, 2015, **85**, 135-146.

38. T. L. Anderson, *Fracture Mechanics: Fundamentals and Applications*, CRC Press, 3 edn., 2005.

Figure

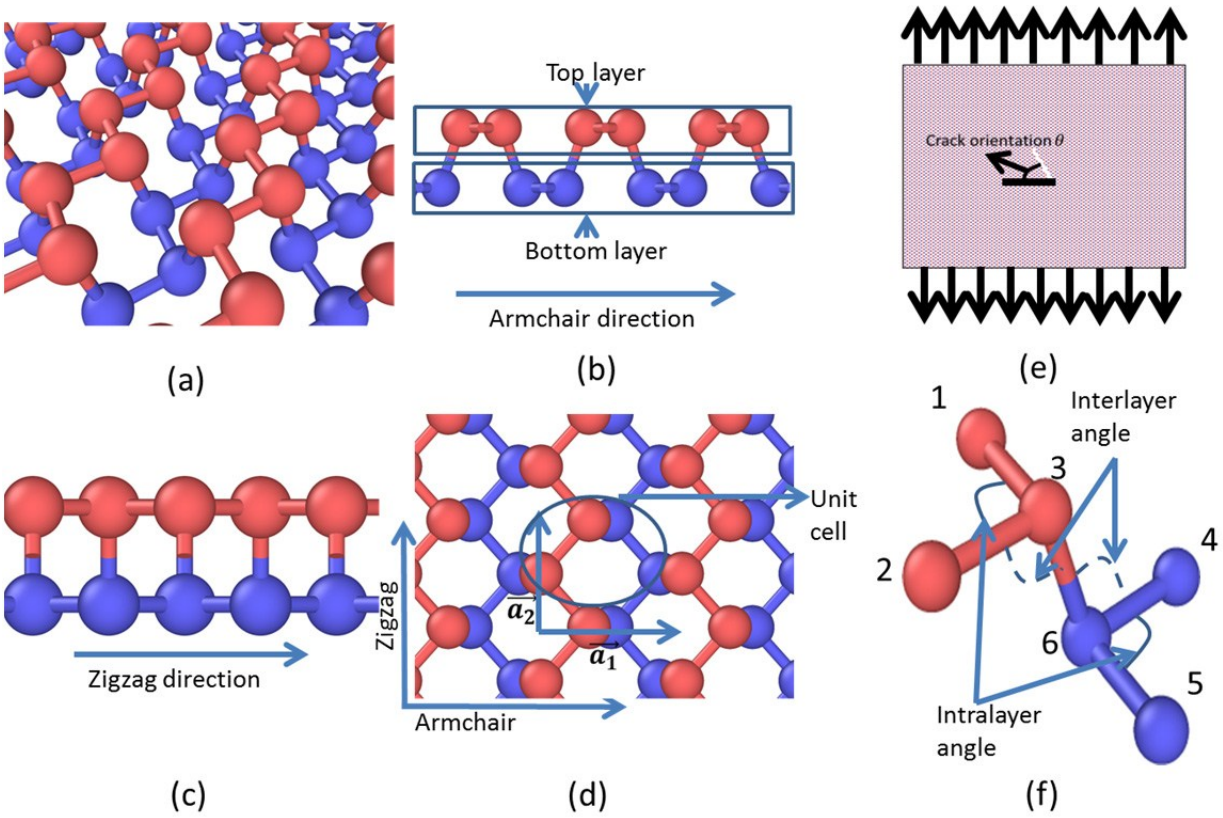

Figure 1 Geometrical configuration of phosphorene: (a) perspective view. Red atoms indicate the atoms on the top layer while blue ones indicate the atoms from the bottom group. (b) side view from the zigzag direction. (c) front view from the armchair direction(d) Top view.$\overrightarrow{a_1}$ and $\overrightarrow{a_2}$ indicate the lattice basis vectors along the armchair and zigzag direction respectively.(e) crack orientation of phosphorene samples(black arrows represent the loading direction; the white line represent a pre-crack) (f) different kinds of angles of phosphorene

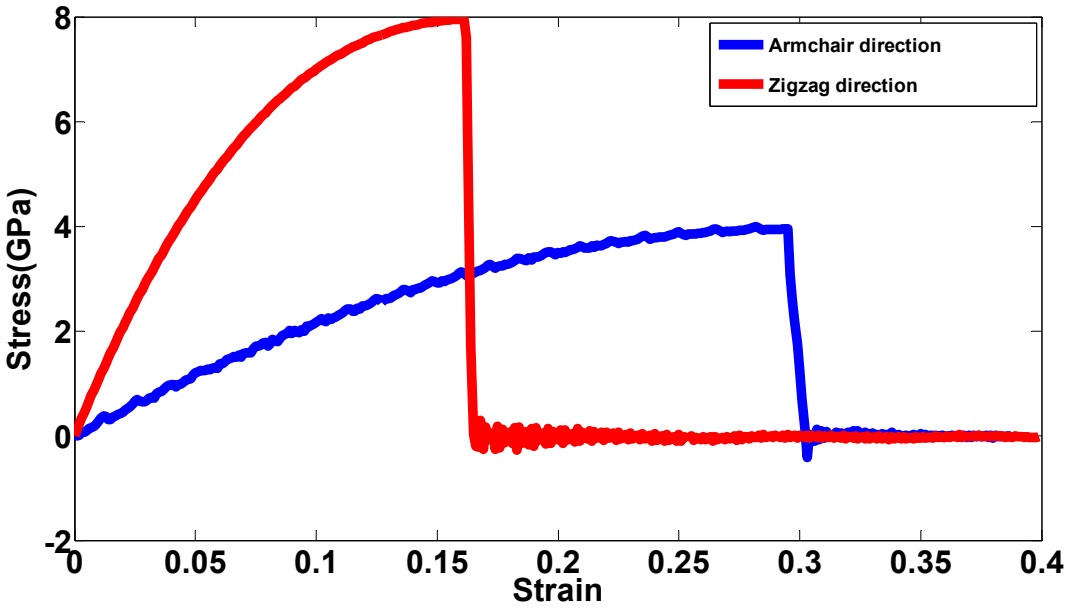

Figure 2 Stress-strain curve of uniaxial tensile tests on pristine samples

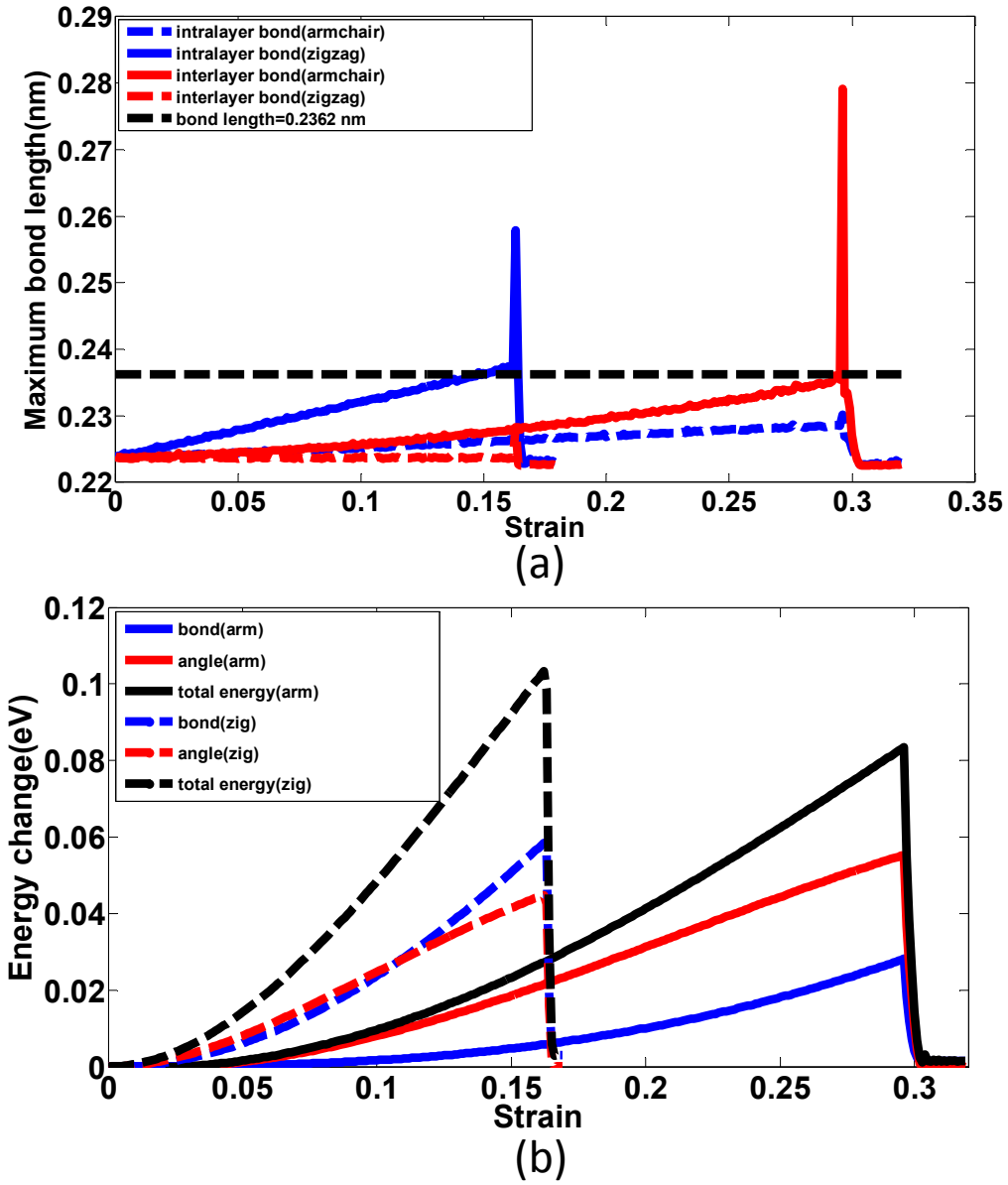

Figure 3 (a) Maximum bond length change (b) Average energy change under uniaxial tension along both armchair and zigzag direction

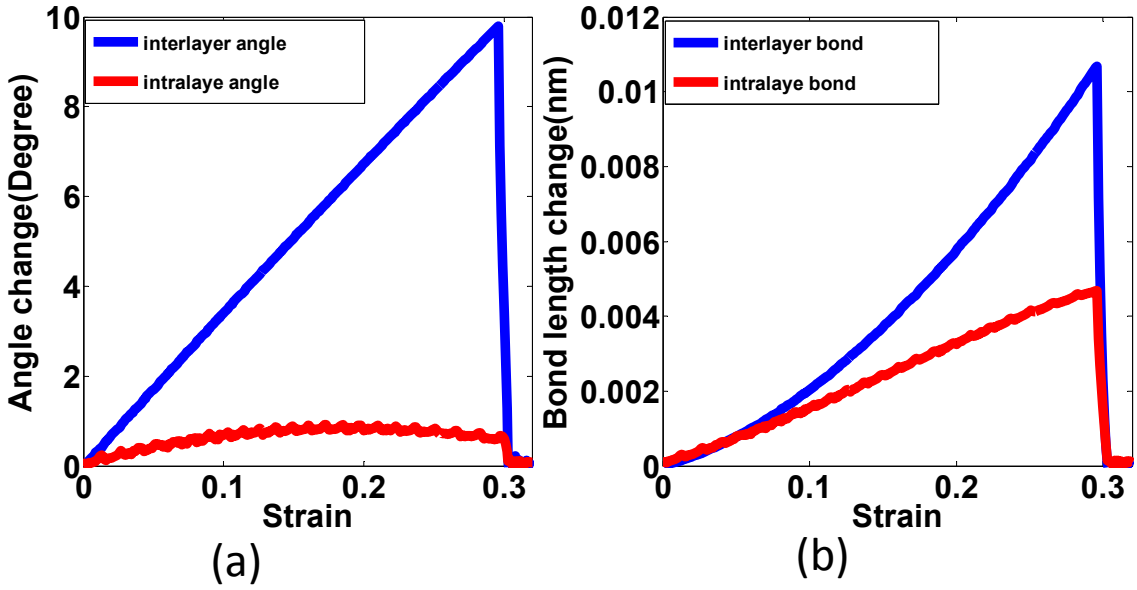

Figure 4 Average angle change and bond length change under uniaxial tension along armchair direction

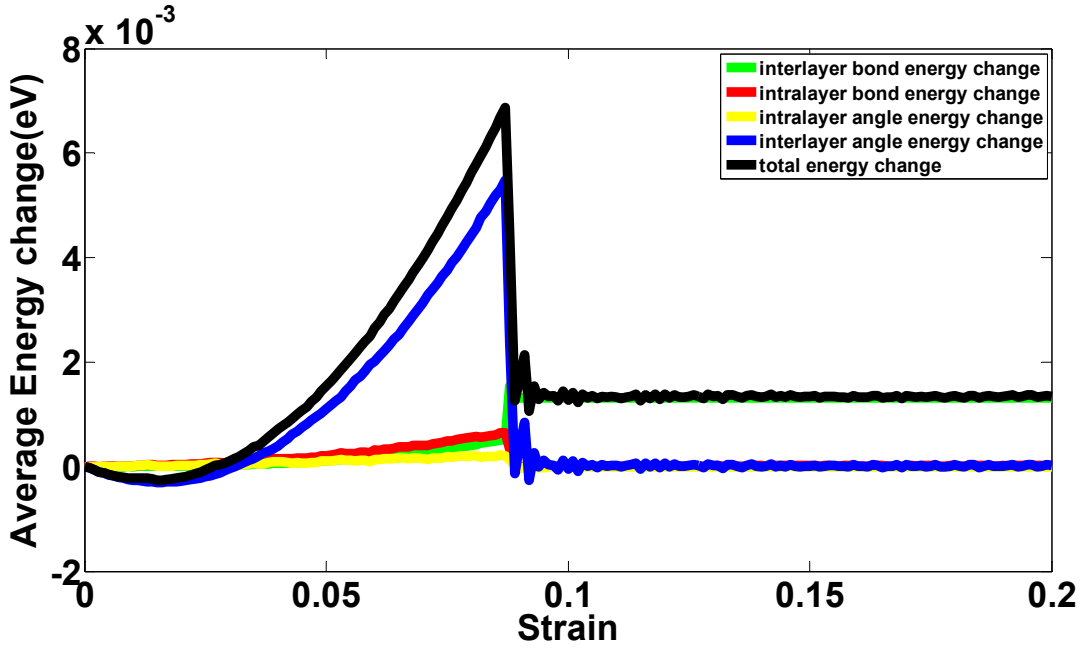

Figure 5 Average energy change during the uniaxial tensile test along the armchair direction

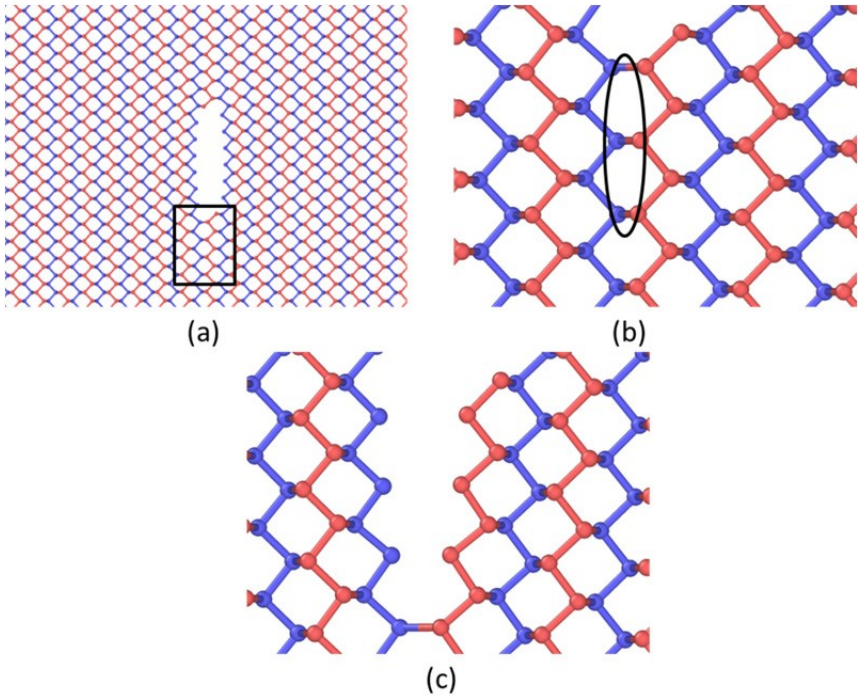

Figure 6 Fracture path under the uniaxial tensile test along armchair direction (a) detailed atomic information around the crack tip before crack propagation (b) zoom-in picture of the black square before propagation (three bonds marked are interlayer bonds)(c) after crack propagation

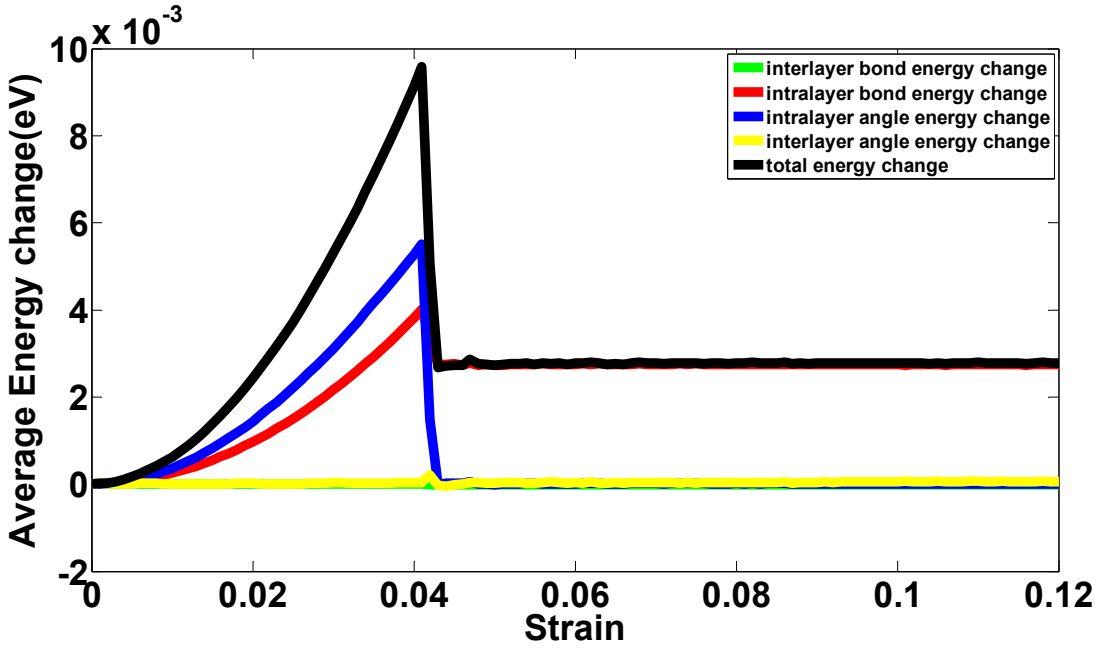

Figure 7 Average energy change during the uniaxial tensile test along the zigzag direction

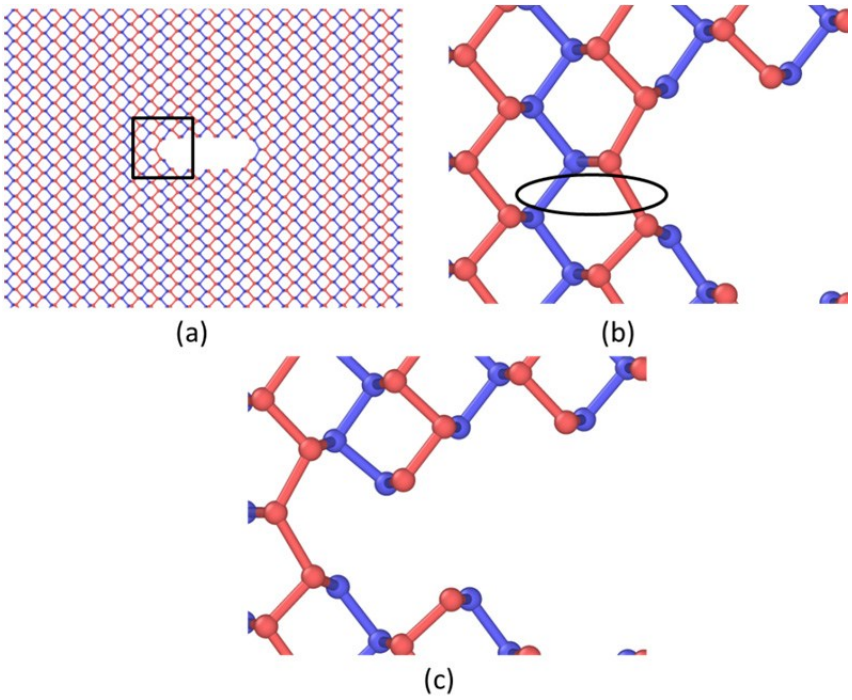

Figure 8 Fracture path under the uniaxial tensile test along zigzag direction (a) detailed atomic information around the crack tip before crack propagation (b) zoom-in picture of the black square before propagation (three bonds marked are intralayer bonds)(c) after crack propagation

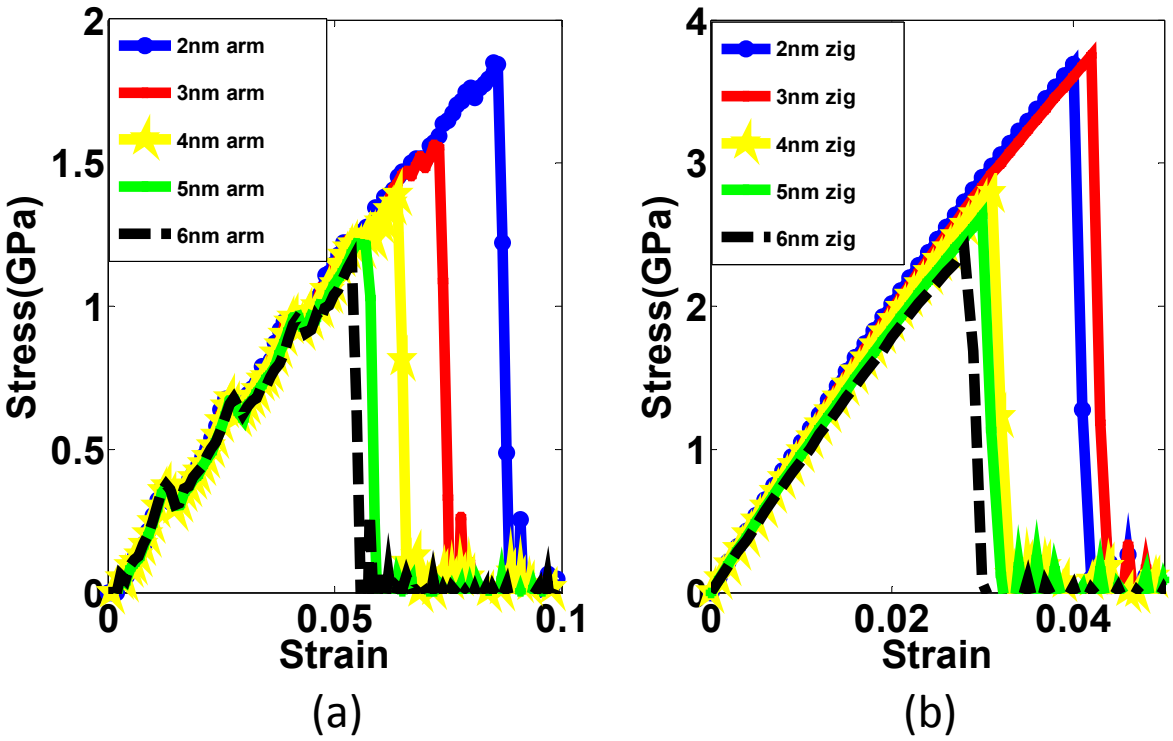

Figure 9 Stress-strain curves of phosphorene with various initial crack length under tension along both armchair direction and zigzag direction (a) armchair direction(Crack orientation Θ is 0^o)(b)zigzag direction(Crack orientation Θ is 0^o)

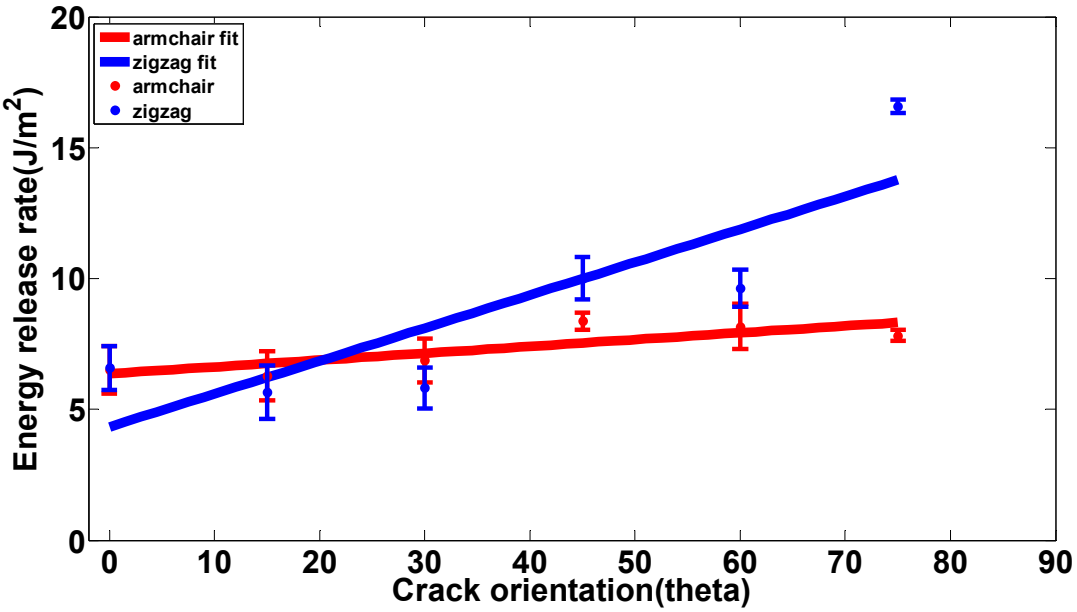

Figure 10 Energy release rate as a function of crack orientation for uniaxial tension along both armchair and zigzag direction

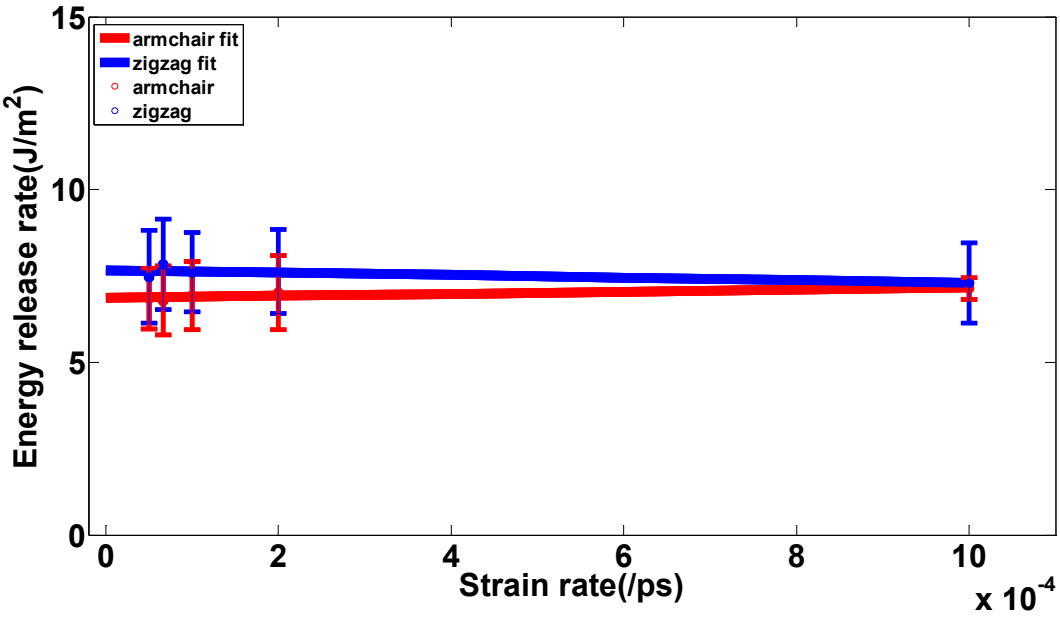

Figure 11 Energy release rate as a function of strain rate for uniaxial tension along both armchair and zigzag direction

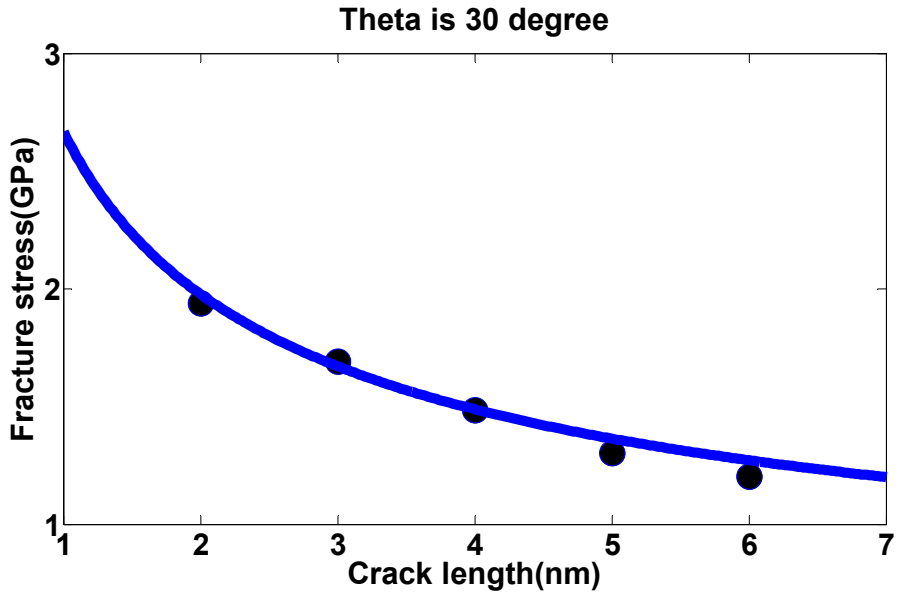

(a) Armchair direction

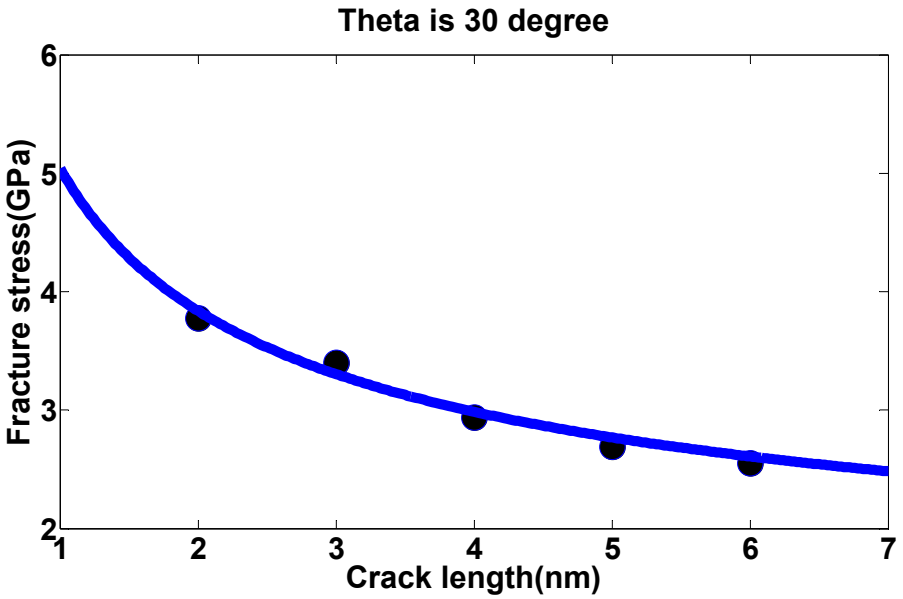

(b)Zigzag direction

Figure 12 Fracture stress versus crack length when crack orientation is 30 degree (a) Armchair direction (b) Zigzag direction (dots represent original data while curves represent fitted results according to Equation 5)

Tables

Table 1 Parameters of the SW potential "tol" represent a controllable parameter of the SW potential form in LAMMPS. Pt represents atoms located on the top layer while Pb represents atoms from the bottom layer.

	$\boldsymbol{\varepsilon}$**(eV)**	$\boldsymbol{\sigma}$**(A)**	a	$\boldsymbol{\lambda}$	$\boldsymbol{\gamma}$	cos$\boldsymbol{\theta_0}$	A	B	p	q	tol
Pt-Pt-Pt	1.000	0.809	3.449	35.701	1.000	-0.111	3.626	33.371	4	0	0.0
Pb-Pb-Pb	1.000	0.809	3.449	35.701	1.000	-0.111	3.626	33.371	4	0	0.0
Pt-Pt-Pb	1.000	0.809	3.449	32.006	1.000	-0.210	0.000	33.371	4	0	0.0
Pb-Pb-Pt	1.000	0.809	3.449	32.006	1.000	-0.210	0.000	33.371	4	0	0.0

Table 2 Geometrical factors α for different crack orientation Θ under both armchair and zigzag unidirectional tensions ($\theta \leq 45^{\circ}$).

Crack orientation	**0**	**15**	**30**	**45**	**Average**	**Standard deviation**
Armchair	0.2282	0.2239	0.2363	0.2214	0.227	0.0057
Zigzag	0.2354	0.2179	0.2221	0.2119	0.222	0.0086